ARTICLE

Modulating Electrical Properties of InAs Nanowires *via* Molecular Monolayers

Ho-Yuen Cheung,[†] SenPo Yip,[‡,§] Ning Han,[∥] Goufa Dong,[‡] Ming Fang,[‡] Zai-xing Yang,[‡,§] Fengyun Wang,[⊥] Hao Lin,[‡] Chun-Yuen Wong,[*,†,§] and Johnny C. Ho[*,‡,§]

[†]Department of Biology and Chemistry, [‡]Department of Physics and Materials Science, and [§]State Key Laboratory of Millimeter Waves, City University of Hong Kong, 83 Tat Chee Avenue, Kowloon, Hong Kong, [∥]State Key Laboratory of Multiphase Complex Systems, Institute of Process Engineering, Chinese Academy of Sciences, Beijing 100190, P.R. China, and [⊥]Cultivation Base for State Key Laboratory, Qingdao University, No. 308 Ningxia Road, Qingdao 266071, P.R. China

ABSTRACT In recent years, InAs nanowires have been demonstrated with the excellent electron mobility as well as highly efficient near-infrared and visible photoresponse at room temperature. However, due to the presence of a large amount of surface states that originate from the unstable native oxide, the fabricated nanowire transistors are always operated in the depletion mode with degraded electron mobility, which is not energy-efficient. In this work, instead of the conventional inorganic sulfur or alkanethiol surface passivation, we employ aromatic thiolate (ArS^-)-based molecular monolayers with controllable molecular design and electron density for the surface modification of InAs nanowires (*i.e.*, device channels) by simple wet chemistry. More importantly, besides reliably improving the device performances by enhancing the electron mobility and the current on–off ratio through surface state passivation, the device threshold voltage (V_{Th}) can also be modulated by varying the *para*-substituent of the monolayers such that the molecule bearing electron-withdrawing groups would significantly shift the V_{Th} towards the positive region for the enhancement mode device operation, in which the effect has been quantified by density functional theory calculations. These findings reveal explicitly the efficient modulation of the InAs nanowires' electronic transport properties *via* ArS^--based molecular monolayers, which further elucidates the technological potency of this ArS^- surface treatment for future nanoelectronic device fabrication and circuit integration.

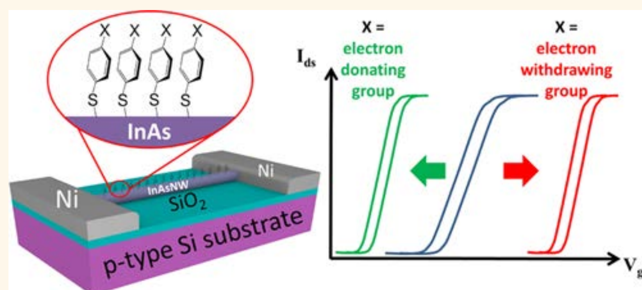

KEYWORDS: InAs nanowires · molecular monolayers · aromatic thiol · threshold voltages · electrical properties · mobility

In past decades, due to their unique physical properties, III–V semiconductor nanowires (NWs) have attracted extensive research and development interests for various technological applications such as electronics, sensors, and photonics.[1–10] In particular, when configured into n-type field-effect transistors (FETs), InAs NWs have been demonstrated with excellent field-effect electron mobility (μ_{FE}) greater than 10 000 $cm^2 V^{-1} s^{-1}$ as well as highly efficient near-infrared and visible photoresponse at room temperature.[11–14] Generally, the device operation in enhancement mode (E-mode), yielding an OFF state at a zero gate bias with a positive threshold voltage (V_{Th}), is highly preferred for the simple, low-power, and large-scale circuit integration design since there is no need to apply gate voltages to switch off the devices.[15,16] However, due to the presence of a large amount of surface states that originate from the unstable native oxide, significant surface trap charges are accumulated on the InAs NW, forming an electron surface accumulation layer, which results in a Fermi level (E_F) pinning above the conduction band.[17,18] This phenomenon would lead to NWFETs operating in the depletion mode (D-mode), where a negative gate bias is required for the device to achieve an OFF state by depleting the accumulated free carriers and is, hence, not energy-efficient.[15,16] Moreover, the electron mobility would also get degraded by the electron scattering induced in this surface accumulation charge layer, especially for the small diameter NWs, due to the large surface-to-volume ratio.[11,12]

In order to tackle the above-mentioned issues, several works have been recently reported that are able to partially solve the problems and can be summarized into two approaches. One technique is that metal

* Address correspondence to johnnyho@cityu.edu.hk, acywong@cityu.edu.hk.

Received for review May 6, 2015 and accepted June 17, 2015.

Published online June 17, 2015
10.1021/acsnano.5b02745

© 2015 American Chemical Society

cluster decoration can be employed to manipulate the device operation by modulating the device's V_{Th} based on the work function difference between the deposited metal clusters and NWs.[19] Another method utilizes the surface chemical passivation of NWs by self-assembly of a sulfur-containing monolayer (SAM), such as ammonium sulfide ($(NH_4)_2S$) or 1-octadecanethiol ($CH_3(CH_2)_{16}CH_2SH$), which is found to enhance the NW device performance by improving the subthreshold swing (SS) and increasing the electron mobility.[20−22] Until now, neither of them has provided the best solution because of their drawbacks. Metal cluster decoration does not cope with the issues of surface states, such that the mobility of decorated nanowires would be inevitably decreased for the E-mode device operation.[19] On the other hand, surface modification with inorganic sulfur or alkanethiols cannot effectively control the device V_{Th} and, thus, the device operation.[21,22] In this regard, with the aim to achieve all of the above requirements, one better approach is to introduce a surface modifier with controllable electron density at the linkage between the modifier and the NW surface, which can improve the mobility by passivating the surface states and at the same time modulate the V_{Th} of NWFETs by varying the electron density of the modifier.

Here, in this work, we design and present a facile and reliable scheme to tailor electronic transport properties of InAs NWs by the surface modification with aromatic thiolate (ArS^-)-based molecular monolayers, instead of the conventional inorganic sulfur or alkanethiols commonly used in the III−V surface passivation. Importantly, when fabricated into FETs, such surface treatment improves the carrier mobility and modulates the device V_{Th} by varying the *para*-substituents of the ArS^- group. It is noted that this ArS^- surface processing can not only decrease the amount of surface traps for the better mobility but also induce the surface electronic charge to move the device V_{Th} positively. Based on the molecular design, applying ArS^- compounds bearing electron-withdrawing groups would result in significant changes that shift the device V_{Th} toward the positive region for the E-mode operation, whereas for ArS^- compounds carrying electron-donating groups, the change in V_{Th} induced by the passivation effect would be eliminated. All of these findings reveal explicitly the efficient modulation of InAs NW electronic transport properties *via* ArS^--based molecular monolayers, which further elucidates the technological potency of this ArS^- surface treatment for future nanoelectronic device fabrication and circuit integration.

RESULTS AND DISCUSSION

For the SAM formation, InAs NWs are first pretreated with 1% HF under nitrogen atmosphere to remove the native surface oxide and to avoid reoxidation.

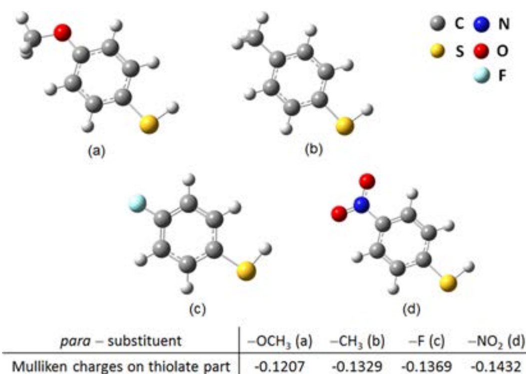

para – substituent	$-OCH_3$ (a)	$-CH_3$ (b)	$-F$ (c)	$-NO_2$ (d)
Mulliken charges on thiolate part	-0.1207	-0.1329	-0.1369	-0.1432

Figure 1. Illustrative schematics of different thiol molecules with various sums of calculated Mulliken charges at the thiolate part of the aromatic thiol derivatives: (a) *p*-methoxythiophenol; (b) *p*-methylthiophenol; (c) *p*-fluorothiophenol; (d) *p*-nitrothiophenol.

Importantly, with the aim to minimize the solvent binding onto the NW surface, isopropyl alcohol (IPA), a branched alcohol, is chosen as the solvent for the aromatic thiol (ArSH) solution; however, since *p*-nitrothiophenol cannot dissolve well in IPA, the solvent is replaced with toluene. It is also noted that the substituent group on the thiol molecules should not have any ability to cross-link with each other and to bind to the NW surface; otherwise, the SAM formation would be uncontrollable. Figure 1 summarizes the chemical structures of all ArSH compounds (*p*-methoxythiophenol ($CH_3O-C_6H_4SH$), *p*-methylthiophenol ($CH_3-C_6H_4SH$), *p*-fluorothiophenol ($F-C_6H_4SH$), and *p*-nitrothiophenol ($NO_2-C_6H_4SH$)) employed in this work as well as the electronic effects of their *para*-substituents affecting the thiol group (represented by the sum of Mulliken charges calculated on the thiolate parts). It is clear that ArS^- with electron-withdrawing groups like the nitro group can decrease the electronic charge on the moiety it bonded to (in this case H), and vice versa for ArS^- with electron-donating groups like the methoxy group.

In order to confirm the monolayer formation, X-ray photoelectron spectroscopy (XPS) is utilized to study the binding nature of the ArS^- compound onto both unpassivated ("before processed") and passivated ("after processed") NWs. $CH_3-C_6H_4SH$ is chosen as the representative compound for the XPS analysis because it is believed that all ArS^- compounds here would have a similar binding nature due to their structural similarity. Moreover, the relatively small shifting of the spectra could be attributed to the size effect as reported in the literature,[23−25] which is not emphasized herein. As shown in Figure 2a, the S 2p binding energy region of the passivated InAs NWs exhibits an obvious peak at ~161.3 eV, indicating that the S atom of the ArS^- group covalently binds to the NWs. In contrast, the unpassivated NWs give no signal there, corresponding to the absence of the thiol molecule attachment. To further investigate the

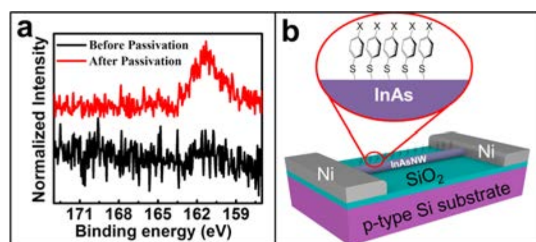

Figure 2. (a) XPS spectra of the S 2p core region obtained from before and after *p*-methylthiophenol-treated InAs nanowires. (b) Illustrated schematic of aromatic thiolate derivatives binding on the surface of the InAs nanowire (the FET channel).

neighboring environment of the S atom, the core level spectra of In 3d and As 3d are also illustrated and analyzed in Supporting Information Figure S1. Considering the In 3d spectra in Figure S1a, we observed the signals of In $3d_{5/2}$ and In $3d_{3/2}$ for both unpassivated and passivated InAs NWs. For the spectrum of unpassivated NWs, In $3d_{5/2}$ peaks (dark line) are fitted with two components for signals at ~444.8 and ~443.9 eV, corresponding to the oxidized In (magenta line) and InAs (olive line). Similar results are also found in In $3d_{3/2}$ peaks, with two components for signals fitted for the oxidized In at ~452.3 eV (magenta line) and for InAs at ~451.4 eV (olive line). When compared to the spectrum of passivated NWs, the relative intensity of oxide signals for passivated NWs is drastically reduced, which indicates the oxide layer being removed after passivation. Moreover, extra peaks are fitted at ~452.1 and ~444.4 eV for passivated NWs, which suggests the establishment of the In−S bond. At the same time, for the As 3d spectra depicted in Figure S1b, the doublet peaks at ~40.2 eV are observed for both unpassivated and passivated NWs, which can be fitted with two components for the signal at ~40.0 and ~40.7 eV, corresponding to the In−As bond. The only difference is that there is an additional peak at ~43.0 eV that appears after passivation, which infers the formation of the As−S bond. Based on these findings, the ArS^- groups are suggested to bind to the NW surface by both In−S and As−S linkages, as illustrated in the schematic in Figure 2b.

Since the electrical performance of InAs NWFETs, such as the electron mobility, V_{Th}, and current on−off ratio ($I_{on/off}$), *etc.*, are known to be significantly degraded by the presence of surface states, especially for small diameter NW channels (<40 nm),[12] the NW channel in the diameter range of 20−30 nm (±2 nm) is purposely chosen in this work in order to investigate the effect of surface modification with ArS^- groups on the NW electrical properties. Furthermore, when we considered the variation induced by the different NW diameter as well as the different amount of surface defects associated with each particular NW device channel, the effect of V_{Th} changes would be assessed in a statistical manner. Specifically, the influence of

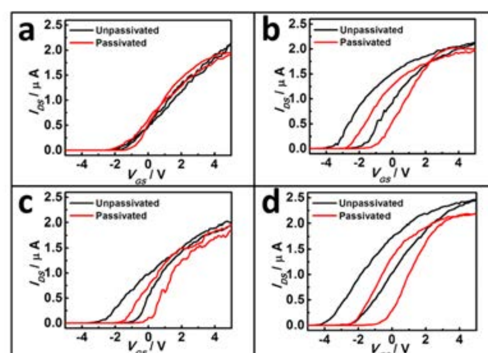

Substitute	-OCH$_3$	-CH$_3$	-F	-NO$_2$
V_{Th} shift / V	0.25 ± 0.23	0.85 ± 0.34	1.00 ± 0.35	1.57 ±0.29

Figure 3. Passivation effect of different aromatic thiolate derivatives on the transfer characteristics of InAs NWFETs: (a) *p*-methoxythiophenol, (b) *p*-methylthiophenol, (c) *p*-fluorothiophenol, and (d) *p*-nitrothiophenol. The magnitude of the V_{Th} shift is calculated based on the average of 21 devices, and the error is constructed by the sample standard deviation.

different *para*-substituents of the ArS^- compound on the transfer characteristics of fabricated NW devices is thoroughly studied and summarized in Figure 3. It is clear that the magnitude of the V_{Th} shift is systematically increased from ~0.25 to ~1.57 V when the substituent is changed from the electron-donating group to the electron-withdrawing group accordingly, indicating that the stronger electron-withdrawing ability of the substituent would lead to the larger V_{Th} shift to the positive region. To further ensure that the V_{Th} changes are induced and originated from the ArS^- group, a control experiment is performed such that the device wafer is placed in the pure solvent under the same condition. It is found that the solvent (*i.e.*, both IPA and toluene) has indeed no significant effect on the V_{Th} change of the NWFET (Supporting Information Figure S2). In addition to the V_{Th} shift demonstrated in the transfer characteristics (Figure 3), the effect of passivation with different ArS^- compounds on other electronic properties of InAs NWFETs, including the $I_{on/off}$, μ_{FE}, and output characteristics, is also studied and presented in Figure 4. Using $CH_3-C_6H_4SH$ passivation as a typical example, the device off current (I_{off}) is drastically reduced while the on current is not changed significantly; consequently, the $I_{on/off}$ is improved after the treatment (Figure 4a). With the statistical data of the $I_{on/off}$ distribution compiled, the passivation could enhance the device $I_{on/off}$ by at least an order of magnitude (Figure 4b). On the other hand, the effect of this passivation on the device's μ_{FE} can be assessed by using the following equation:

$$\mu_{FE} = GL^2/C_{ox} \cdot V_{ds}$$

where G is the transconductance (dI_{ds}/dV_{gs}), L is the NW channel length, C_{ox} is the gate oxide capacitance, and V_{ds} is the drain voltage.

As depicted in Figure 4c, the typical electron mobility is found to slightly increase from ∼3000 to ∼3300 $cm^2 V^{-1} s^{-1}$, which is attributed to the reduced scattering of charge carriers by the removal of surface states, consistent with the $CH_3(CH_2)_{16}CH_2SH$ passivation reported in the literature.[22] In addition, after the passivation, the NW devices remain operating in ohmic behavior, as illustrated in the output characteristics ($I_{ds}-V_{ds}$ curves) in Figure 4d, which indicates that the passivation process has no adverse effect on the contact properties of these NW devices. Besides the $CH_3-C_6H_4SH$ compound, the passivating effects of other ArS^- derivatives and $CH_3(CH_2)_{16}CH_2SH$ on NW devices are also examined, which give similar results as shown in the Supporting Information (Figure S3−S5). Notably, the effect of these monolayers on the electrical properties of NW devices could still be observed after 1 month of storage in vacuum, indicating the stability of these monolayers and their versatility for device applications. To summarize, using the ArS^- surface passivation, the V_{Th} of FETs can be modulated accordingly by varying the *para*-substituent with other electrical properties (*i.e.*, I_{off}, $I_{on/off}$, and μ_{FE}) simultaneously improved. A brief comparison of the effects on NW electrical properties with other device treatments is shown in Table 1.

To shed light on the fundamental effects of different ArS^- groups on the electrical properties of NWs, density functional theory (DFT) calculations are also performed for all ArS^- compounds bonded to the InAs (100) surface, employing the ONIOM (our own *N*-layer integrated molecular orbital molecular mechanics) calculation, and the full model is given in the Supporting Information Figures S6−S9. Since the electronic transport properties of NWs are surface-dominant,[12,22] only the surface layer of InAs and the thiolate part are treated at the DFT level, and the inner layer of the InAs is treated with the force field (UFF) calculation to reduce computational cost. The illustrative schematic is shown in Figure 5a, assuming the thiolate is directly attached onto the InAs surface *via* the As−S linkage. To quantify the electronic effect of various substituents of the ArS^- group, the Mulliken charges of all atoms treated at the DFT level are calculated and used to characterize the electron density distribution. As the charge value becomes more negative, the higher electron density distributed at that particular atom is represented. This way, the electronic effect of various ArS^- passivations on the V_{Th} of NWFETs can be evaluated by summing the Mulliken charges of the atoms belonging to the thiolate part, as described in Figure 5b. Moreover, due to the size effect of the employed molecules for the monolayer formation, the estimated molecular footprints for each particular thiolate attached onto both In- and As-terminated surfaces (Supporting Information Figures S10 and S11) are also demonstrated, which indicate that the impact of this size effect is insignificant here. It is clearly observed that the stronger electron-withdrawing ability results in the larger magnitude of the V_{Th} shift toward the positive value.

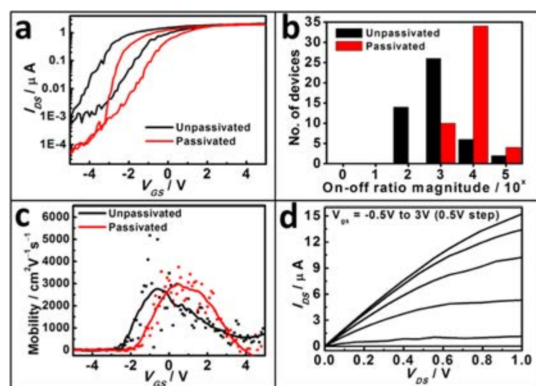

Figure 4. Passivation effect of 4-methylthiophenol on other electronic transport properties of InAs NWFETs including $I_{ds}-V_{gs}$ curves in the log scale (a), device I_{on}/I_{off} ratio distributions of 48 samples (b), mobility changes represented by the fitting curve of the data points using the Savitzky−Golay filter method (c), and $I_{ds}-V_{ds}$ curves after the passivation (d).

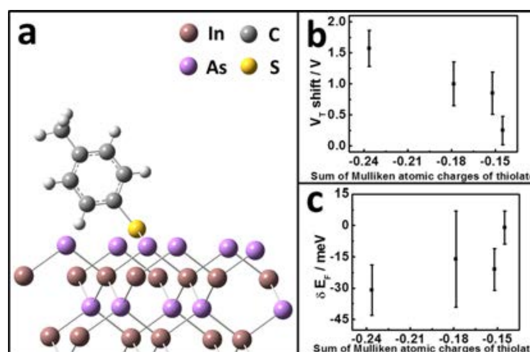

Figure 5. Model for the structurally optimized $CH_3-C_6H_4S^-$-attached InAs (100) surface *via* the S−As linkage (a). Distributions of the V_{Th} shift with different calculated Mulliken atomic charge (b). Mean of the change of Fermi energy of 30 different passivated NW samples with different calculated Mulliken atomic charges. The error refers to the standard deviation of the mean (c).

TABLE 1. Comparison of the Effects on NW Electrical Properties Using Different Passivation/Decoration Approaches

effect on NW electrical properties	alkanethiol passivation	metal cluster decoration[19]	aromatic thiol passivation
V_{Th} shift	constant value	Au: +3.2 V	range from +0.25 to +1.57 V
μ_{FET} change	∼+1000 $cm^2 V^{-1} s^{-1}$	Au: −1200 $cm^2 V^{-1} s^{-1}$	range from +300 to +2000 $cm^2 V^{-1} s^{-1}$
$I_{on/off}$	increase an order of magnitude		increase an order of magnitude

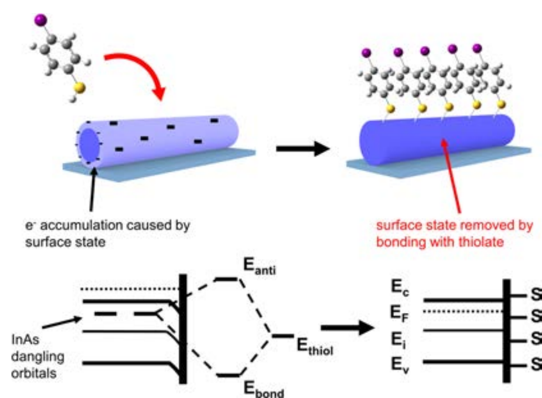

Figure 6. Illustrative schematic and the corresponding band diagrams showing the surface passivation effect on NWs by the thiol molecules.

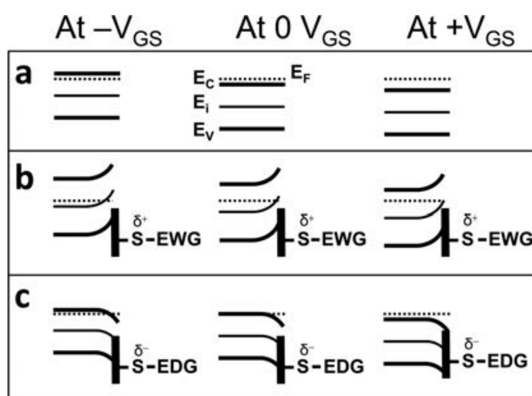

Figure 7. Energy band diagrams of different ArS^- surface treatments on InAs NWs at different gate biases: (a) bare InAs NW channel without any passivation, (b) passivated with the thiol bearing electron-withdrawing groups (EWG), (c) passivated by the thiol bearing electron-donating groups (EDG).

In addition to the V_{Th} modulation, various changes of the free carrier concentration, n, before and after the ArS^- passivation are approximated and illustrated in the Supporting Information Figure S12. Considering the carrier concentration at the position of zero gate bias ($V_{gs} = 0$), we found that the deposited ArS^- group bearing the stronger electron-withdrawing group gives a larger decrease of carrier concentration, which suggests that a large amount of carriers are depleted from the InAs surface, resulting in a depletion layer and reduction of the effective channel width of the NW. Using the above results, the changes of E_F of InAs NWs due to the electronic effect of different ArS^- groups can be estimated by the following equation:

$$\frac{n_A}{n_B} = \exp\left(\frac{E_{FA} - E_{FB}}{kT}\right)$$

where k is the Boltzmann constant, T is the temperature, subscript A and B refer to the case after and before the passivation, statistically summarized in Figure 5c, similar to the determination of V_{Th} changes as discussed above. Similar consistent results are also observed for the calculations with the thiolate directly attached onto the InAs surface *via* the In−S linkage (Supporting Information Figure S13). It is clear that the electron-withdrawing ability of the deposited ArS^- group is approximately proportional to the decrease of the E_F of NWs, demonstrating the reliable control of NW electrical properties *via* this simple ArS^- passivation technique.

Based on all of these findings, we can see that the NW surface modification with ArS^- groups provides both passivation effect and V_{Th} modulation ability of the InAs NWFETs. Figure 6 shows a schematic illustrating the corresponding change of the band diagram of InAs NWs induced by the passivation effect. For the unpassivated NWs, the existing surface defects typically lead to the formation of dangling orbitals, which locate near the conduction band.[26] These orbitals would then induce the interface trap charges on the NW surface and contribute to an electron accumulation layer, which gives rise to the Fermi level (E_F) being pinned near or above the conduction band edge.[17,18] It should also be noted that such an electron-rich layer increases the charge carrier scattering and reduces the mobility during the electrical conduction and, at the same time, yields a significant leakage current in the device OFF state. Nevertheless, after the passivation, some of the dangling orbitals are passivated by the As−S and In−S linkages, and the electron concentration of the accumulation layer would be decreased accordingly (*i.e.*, carrier depletion), which results in shifting the E_F below the conduction band, considering that the depletion extends over the entire volume of these thin NWs.[27] As a result, the corresponding charge carrier scattering is minimized with the electron mobility improved and the I_{off} of the NWFETs reduced. Since the I_{on} is mainly limited by the contact resistance, no significant change is expected to be observed here. To further investigate the physical mechanism of this NW electrical property modulation by ArS^- modification, Figure 7 depicts the energy band diagrams of NWs modified with ArS^- groups bearing different electron-donating and electron-withdrawing groups at different gate biases. As mentioned above, in the equilibrium state ($V_{gs} = 0$ V), the prepared InAs NWs are intrinsically n-type with the E_F lying near or slightly pinned above the conduction band edge; therefore, a negative gate bias is required to move the bands up or push the E_F down in order to deplete the excess electrons to achieve the device OFF state, which is known as the D-mode device operation (Figure 7a). In contrast, as shown in Figure 7b, when the ArS^- groups bearing electron-withdrawing groups (*i.e.*, $F-C_6H_4S^-$ and $NO_2-C_6H_4S^-$) bonded onto the NW channel surface, the electron-withdrawing ability of the substituent would locally disturb the energy band to bend upward at the NW/S interface such that the free electrons are depleted to move the E_F down to the

intrinsic level at V_{gs} = 0 V. Combining the passivation effect, the current at the zero gate bias would be drastically reduced nearly to zero unless a small positive gate bias is introduced to pull the band down, inducing a large current given by the high concentration of carriers, in which the device is performed in the E-mode operation. Similarly, when the ArS^- bearing electron-donating groups (*i.e.*, $CH_3-C_6H_4S^-$ and $MeO-C_6H_4S^-$) bonded on the NW surface, the substituent effect would show the energy band locally bending downward at the NW/S interface and move the E_F up to the conduction band. This would lead to the reduction or even calling off the effect of ArS^- passivation on the E_F shifting (Figure 6), which results in the V_{Th} moving slightly to the positive region or remaining unchanged. Since this band model is only presented qualitatively, more theoretical models are required to further quantify the effect. In any case, all of these demonstrated the versatility of this simple ArS^- surface treatment in modulating NW electrical properties for the realization of high-performance nanoelectronic devices and circuits.

CONCLUSIONS

In summary, we have demonstrated a simple and reliable approach to tailor the device operation of InAs NWFETs *via* molecular monolayers, which can improve the device performance as well as effectively modulate the device V_{Th} by varying the *para*-substituents of the ArS^- groups. Specifically, deposition of the ArS^- groups can reduce the NW surface states *via* surface passivation, and the electron concentration trapped in this surface-state-induced accumulation layer would decrease accordingly, which minimizes the carrier scattering for better mobility and reduces the leakage current in the device OFF state for better $I_{on/off}$. More importantly, the device V_{Th} can be increased reliably by changing the *para*-substituents from electron-donating groups to electron-withdrawing groups and *vice versa*. These findings reveal explicitly the efficient modulation of InAs NW electronic transport properties *via* ArS^--based molecular monolayers, which further elucidates the technological potency of this ArS^- surface treatment for future nanoelectronic device fabrication and circuit integration.

METHODS

InAs NWFET Fabrication. The InAs NWs used in this study were prepared by a solid-source catalytic chemical vapor deposition method as previously reported.[28] Briefly, about 1.2 g of InAs powders (99.9999% purity) was heated to 690 °C in the upstream zone of a two-zone tube furnace, and the evaporated precursors were transported by the H_2 carrier gas (200 sccm) to the downstream zone at a temperature of 470 °C. In this zone, InAs NWs were grown utilizing the 0.2 nm thick Ni catalyst film (preannealed at 800 °C for 10 min) predeposited on SiO_2/Si substrates for 60 min. The pressure was maintained at ~1.0 Torr. After being cooled in the H_2 gas atmosphere, the grown NWs were harvested in anhydrous ethanol by sonication and then drop-casted onto SiO_2/Si substrates (50 nm thermally grown oxide on degenerately boron-doped Si) for the fabrication of back-gated FETs. In this study, NWFETs were achieved by the definition of electrodes using a standard lithography process, followed by the deposition of 50 nm thick Ni and subsequent metal lift off.

SAM of ArS^- Compound Preparation. The passivation of InAs NWs after device fabrication (*i.e.*, the FET channel) was prepared under N_2 atmosphere with the following procedures. The device wafer was first treated by HF (1%) solution for 6 s, rinsed by deionized water, and then placed into the freshly prepared 35 mM IPA solution of $MeO-C_6H_4SH$, $CH_3-C_6H_4SH$, or $F-C_6H_4SH$ or toluene solution of $NO_2-C_6H_4SH$ at room temperature for 12 h. After being removed from the solution, the wafer was rinsed with ethanol and blown dry with nitrogen. For the XPS analysis, the ArS^--passivated NWs were prepared by the above procedure, except for putting the grown NW substrates, instead of the device wafer, into the solution.

Material and Electrical Characterization. InAs NWs before and after the ArS^- surface passivation were characterized by XPS (Thermo Scientific, ESCALAB 250) with monochromatic Al Kα radiation at a constant analyzer pass energy of 30 eV for high-resolution spectra and 100 eV for survey spectra. The room temperature electrical performances of the fabricated back-gated NWFETs were characterized with a standard electrical probe station connected with a semiconductor analyzer (Agilent 4155C). The diameters and channel length for all NW channels of the FETs were subsequently characterized by scanning electron microscopy (FEI Company, Oregon, USA/Philips XL30, Philips Electronics, Amsterdam, The Netherlands).

Computational Methodology. The ONIOM[29] method was performed for calculations of the charge distribution of all ArS^- compounds adsorbed on the InAs (100) surface. Specifically, the calculation models were separated into two layers. The "top" layer included the ArS^- compound, with the atomic layer attached, and the electronic ground states of ArS^- compounds were optimized without symmetry imposed using various DFT methods (generalized gradient approximation of Becke[30] and Perdew[31] exchange−correlation functional (BP86) for the structural optimization; Becke's three-parameter hybrid functional[32] with the Lee−Yang−Parr correlation functional[33] (B3LYP) for electronic energies, and Mulliken charge calculations); frequency calculations on the optimized structures were also performed to confirm their nature as local minima. The 6-31G(d) (for structural optimization) and 6-311+G(2df,p) (for electronic energies and Mulliken charge calculations) basis sets were employed for C, H, N, O, F, and S atoms.[34−38] The Dunning−Huzinaga valence double-zeta with the Los Alamos effective core potential plus double-zeta basis set (LanL2DZ) was exploited for In and As atoms.[39−42] The "bottom" layer was modeled by molecular mechanics using the universal force field (UFF).[43] All In and As atoms were calculated without optimization using the geometry of X-ray crystal structure.[44] Mulliken charge was used to interpret the charge distribution in all cases. All DFT calculations were performed using the Gaussian 09 program package (revision B.01).[45]

Conflict of Interest: The authors declare no competing financial interest.

Acknowledgment. This research is supported by the Research Grants Council of Hong Kong SAR, China (CityU 103911 and CityU 139413), the National Natural Science Foundation of China (Grant No. 51402160), and the State Key Laboratory of Multiphase Complex Systems (MPCS-2014-C-01).

Supporting Information Available: XPS analysis of In 3d spectra and As 3d spectra for before and after *p*-methylthiophenol-treated InAs nanowires, control experiments and passivation effects of other ArS^- derivatives on the electronic transport properties, calculation models of ArS^- derivatives

binding on the InAs clusters, molecular footprint for aromatic thiolate derivatives attached to both In and As atoms on the InAs surface, and the estimated carrier concentrations. The Supporting Information is available free of charge on the ACS Publications website at DOI: 10.1021/acsnano.5b02745.

REFERENCES AND NOTES

1. Van, W. I.; Plissard, S. R.; Bakkers, E. P. A. M.; Frolov, S. M.; Kouwenhoven, L. P. Quantized Conductance in an InSb Nanowire. *Nano Lett.* **2013**, *13*, 387–391.
2. Hou, J. J.; Han, N.; Wang, F.; Xiu, F.; Yip, S. P.; Hui, A. T.; Hung, T. F.; Ho, J. C. Synthesis and Characterizations of Ternary InGaAs Nanowires by a Two-Step Growth Method for High-Performance Electronic Devices. *ACS Nano* **2012**, *6*, 3624–3630.
3. Wallentin, J.; Ek, M.; Wallenberg, L. R.; Samuelson, L.; Borgström, M. T. Electron Trapping in InP Nanowire FETs with Stacking Faults. *Nano Lett.* **2012**, *12*, 151–155.
4. Wu, P. M.; Anttu, N.; Xu, H. Q.; Samuelson, L.; Pistol, M. E. Colorful InAs Nanowire Arrays: From Strong to Weak Absorption with Geometrical Tuning. *Nano Lett.* **2012**, *12*, 1990–1995.
5. Yang, Z.-X.; Han, N.; Fang, M.; Lin, H.; Cheung, H.-Y.; Yip, S. P.; Wang, E.-J.; Hung, T. F.; Wong, C.-Y.; Ho, J. C. Surfactant-Assisted Chemical Vapour Deposition of High-Performance Small-Diameter GaSb Nanowires. *Nat. Commun.* **2014**, *5*, 5249.
6. Tomioka, K.; Yoshimura, M.; Fukui, T. A III−V Nanowire Channel on Silicon for High-Performance Vertical Transistors. *Nature* **2012**, *488*, 189–192.
7. del Alamo, J. A. Nanometre-Scale Electronics with III−V Compound Semiconductors. *Nature* **2011**, *479*, 317–323.
8. Ionescu, A. M.; Riel, H. Tunnel Field-Effect Transistors as Energy-Efficient Electronic Switches. *Nature* **2011**, *479*, 329–337.
9. Spirkoska, D.; Fontcuberta i Morral, A.; Dufouleur, J.; Xie, Q.; Abstreiter, G. Free Standing Modulation Doped Core−Shell GaAs/AlGaAs Hetero-Nanowires. *Phys. Status Solidi RRL* **2011**, *5*, 353–355.
10. Gudiksen, M. S.; Lauhon, L. J.; Wang, J.; Smith, D. C.; Lieber, C. M. Growth of Nanowire Superlattice Structures for Nanoscale Photonics and Electronics. *Nature* **2002**, *415*, 617–620.
11. Thelander, C.; Caroff, P.; Plissard, S.; Dey, A. W.; Dick, K. A. Effects of Crystal Phase Mixing on the Electrical Properties of InAs Nanowires. *Nano Lett.* **2011**, *11*, 2424–2429.
12. Ford, A. C.; Ho, J. C.; Chueh, Y. L.; Tseng, Y. C.; Fan, Z. Y.; Guo, J.; Bokor, J.; Javey, A. Diameter-Dependent Electron Mobility of InAs Nanowires. *Nano Lett.* **2009**, *9*, 360–365.
13. Schroer, M. D.; Petta, J. R. Correlating the Nanostructure and Electronic Properties of InAs Nanowires. *Nano Lett.* **2010**, *10*, 1618–1622.
14. Guo, N.; Hu, W.; Liao, L.; Yip, S. P.; Ho, J. C.; Miao, J.; Zhang, Z.; Zou, J.; Jiang, T.; Wu, S.; et al. Anomalous and Highly Efficient InAs Nanowire Phototransistors Based on Majority Carrier Transport at Room Temperature. *Adv. Mater.* **2014**, *26*, 8203–8209.
15. Xuan, Y.; Wu, Y. Q.; Ye, P. D. High-Performance Inversion-Type Enhancement-Mode InGaAs MOSFET with Maximum Drain Current Exceeding 1 A/mm. *IEEE Electron Device Lett.* **2008**, *29*, 294–296.
16. Zou, X.; Liu, X.; Wang, C.; Jiang, Y.; Wang, Y.; Xiao, X.; Ho, J. C.; Li, J.; Jiang, C.; Xiong, Q. H.; et al. Controllable Electrical Properties of Metal-Doped In_2O_3 Nanowires for High-Performance Enhancement-Mode Transistors. *ACS Nano* **2013**, *7*, 804–810.
17. Tsui, D. C. Observation of Surface Bound State and Two-Dimensional Energy Band by Electron Tunneling. *Phys. Rev. Lett.* **1970**, *24*, 303–306.
18. Olsson, L. Ö.; Andersson, C. B. M.; Håkansson, M. C.; Kanski, J.; Ilver, L.; Karlsson, U. O. Charge Accumulation at InAs Surfaces. *Phys. Rev. Lett.* **1996**, *76*, 3626–3629.
19. Han, N.; Wang, F.; Hou, J. J.; Yip, S. P.; Lin, H.; Xiu, F.; Fang, M.; Yang, Z.; Shi, X.; Dong, G.; et al. Tunable Electronic Transport Properties of Metal-Cluster-Decorated III−V Nanowire Transistors. *Adv. Mater.* **2013**, *25*, 4445–4451.
20. Petrovykh, D. Y.; Yang, M. J.; Whitman, L. J. Chemical and Electronic Properties of Sulfur-Passivated InAs Surfaces. *Surf. Sci.* **2003**, *523*, 231–240.
21. Suyatin, D. B.; Thelander, C.; Björk, M. T.; Maximov, I.; Samuelson, L. Sulfur Passivation for Ohmic Contact Formation to InAs Nanowires. *Nanotechnology* **2007**, *18*, 105307.
22. Hang, Q.; Wang, F.; Carpenter, P. D.; Zemlyanov, D.; Zakharov, D.; Stach, E. A.; Buhro, W. E.; Janes, D. B. Role of Molecular Surface Passivation in Electrical Transport Properties of InAs Nanowires. *Nano Lett.* **2008**, *8*, 49–55.
23. Johnson, D. C.; Benfield, R. E.; Edwards, P. P.; Nelson, W. J. H.; Vargas, M. D. Study of Magnetism in Osmium Cluster Compounds as Molecular Models for Small Metallic Particles. *Nature* **1985**, *314*, 231–235.
24. Rao, C. N. R.; Kulkarni, G. U.; Thomas, P. J.; Edwards, P. P. Size-Dependent Chemistry: Properties of Nanocrystals. *Chem.—Eur. J.* **2002**, *8*, 28–35.
25. Volokitin, Y.; Sinzig, J.; de Jongh, L. J.; Schmid, G.; Vargaftik, M. N.; Moiseev, I. I. Quantum-Size Effects in the Thermodynamic Properties of Metallic Nanoparticles. *Nature* **1996**, *384*, 621–623.
26. Gerischer, H. On the Role of Electrons and Holes in Surface Reactions on Semiconductors. *Surf. Sci.* **1969**, *13*, 265–278.
27. Han, N.; Wang, F. Y.; Hou, J. J.; Xiu, F.; Yip, S. P.; Hui, A. T.; Hung, T. F.; Ho, J. C. Controllable p-n Switching Behaviors of GaAs Nanowires *via* an Interface Effect. *ACS Nano* **2012**, *6*, 4428–4433.
28. Wang, F. Y.; Yip, S. P.; Han, N.; Fok, K. W.; Lin, H.; Hou, J. J.; Dong, G.; Hung, T. F.; Chan, K. S.; Ho, J. C. Surface Roughness Induced Electron Mobility Degradation in InAs Nanowire. *Nanotechnology* **2013**, *24*, 375202.
29. Svensson, M.; Humbel, S.; Froese, R. D. J.; Matsubara, T.; Sieber, S.; Morokuma, K. ONIOM: A Multilayered Integrated MO+MM Method for Geometry Optimizations and Single Point Energy Predictions. A Test for Diels−Alder Reactions and $Pt(P(t\text{-}Bu)_3)_2 + H_2$ Oxidative Addition. *J. Phys. Chem.* **1996**, *100*, 19357–19363.
30. Becke, A. D. Density-Functional Exchange-Energy Approximation with Correct Asymptotic Behavior. *Phys. Rev. A* **1988**, *38*, 3098–3100.
31. Perdew, J. P. Density-Functional Approximation for the Correlation Energy of the Inhomogeneous Electron Gas. *Phys. Rev. B* **1986**, *33*, 8822–8824.
32. Becke, A. D. Density-Functional Thermochemistry. III. The Role of Exact Exchange. *J. Chem. Phys.* **1993**, *98*, 5648–5652.
33. Lee, C.; Yang, W.; Parr, R. G. Development of the Colle-Salvetti Correlation-Energy Formula into a Functional of the Electron Density. *Phys. Rev. B* **1988**, *37*, 785–789.
34. Hehre, W. J.; Ditchfield, R.; Pople, J. A. Self-Consistent Molecular Orbital Methods. XII. Further Extensions of Gaussian-Type Basis Sets for Use in Molecular Orbital Studies of Organic Molecules. *J. Chem. Phys.* **1972**, *56*, 2257–2261.
35. Francl, M. M.; Pietro, W. J.; Hehre, W. J.; Binkley, J. S.; Gordon, M. S.; DeFrees, D. J.; Pople, J. A. Self-Consistent Molecular Orbital Methods. XXIII. A Polarization-Type Basis Set for Second-Row Elements. *J. Chem. Phys.* **1982**, *77*, 3654–3665.
36. McLean, A. D.; Chandler, G. S. Contracted Gaussian Basis Sets for Molecular Calculations. I. Second Row Atoms, $Z=11-18$. *J. Chem. Phys.* **1980**, *72*, 5639–5648.
37. Clark, T.; Chandrasekhar, J.; Spitznagel, G. W.; Schleyer, P. V. R. Efficient Diffuse Function-Augmented Basis Sets for Anion Calculations. III. The 3-21+G Basis Set for First-Row Elements, Li−F. *J. Comput. Chem.* **1983**, *4*, 294–301.
38. Frisch, M. J.; Pople, J. A.; Binkley, J. S. Self-Consistent Molecular Orbital Methods 25. Supplementary Functions for Gaussian Basis Sets. *J. Chem. Phys.* **1984**, *80*, 3265–3269.
39. Dunning, T. H., Jr.; Hay, P. J. Gaussian Basis Sets for Molecular Calculations. In *Methods of Electronic Structure*

Theory; Schaefer, H. F., III, Ed.; Springer: New York, 1977; pp 1−27.
40. Hay, P. J.; Wadt, W. R. Ab Initio Effective Core Potentials for Molecular Calculations. Potentials for the Transition Metal Atoms Sc to Hg. *J. Chem. Phys.* **1985**, *82*, 270–283.
41. Wadt, W. R.; Hay, P. J. Ab Initio Effective Core Potentials for Molecular Calculations. Potentials for Main Group Elements Na to Bi. *J. Chem. Phys.* **1985**, *82*, 284–298.
42. Hay, P. J.; Wadt, W. R. Ab Initio Effective Core Potentials for Molecular Calculations. Potentials for K to Au Including the Outermost Core Orbitals. *J. Chem. Phys.* **1985**, *82*, 299–310.
43. Rappé, A. K.; Casewit, C. J.; Colwell, K. S.; Goddard, W. A., III; Skiff, W. M. UFF, a Full Periodic Table Force Field for Molecular Mechanics and Molecular Dynamics Simulations. *J. Am. Chem. Soc.* **1992**, *114*, 10024–10035.
44. Iandelli, A. Sulla Struttura Dei Composti In P, In As e In Sb. *Gazz. Chim. Ital.* **1940**, *70*, 58–62.
45. Frisch, M. J.; Trucks, G. W.; Schlegel, H. B.; Scuseria, G. E.; Robb, M. A.; Cheeseman, J. R.; Scalmani, G.; Barone, V.; Mennucci, B.; Petersson, G. A.; et al. *Gaussian 09*, revision B.01; Gaussian, Inc.: Wallingford, CT, 2009.